Available online at www.sciencedirect.com
SCIENCE DIRECT®
Journal of Membrane Science 262 (2005) 117–128
journal of MEMBRANE SCIENCE
www.elsevier.com/locate/memsci

Simulation of heat and mass transfer in direct contact membrane distillation (MD): The effect of membrane physical properties

A.O. Imdakm*, T. Matsuura

Industrial Membrane Research Center, Department of Chemical Engineering, University of Ottawa, Ont., Canada K1N 6N5

Received 11 April 2005; received in revised form 11 April 2005; accepted 12 May 2005

Abstract

A Monte Carlo simulation model is developed to study vapor flux through hydrophobic membranes in association with direct contact membrane distillation (DCMD) process. The porous membrane is represented by a three-dimensional network model of inter-connected cylindrical pores with distributive effective pore sizes. Vapor flux through membrane pores is described by gas transport mechanisms founded on the kinetic theory of gases for a single cylindrical pore. This model can take into consideration the effects of temperature polarization phenomenon, porous membrane physical properties, including membrane pores inter-connectivity (topology), process dynamics, and apply them into the prediction of process vapor flux (permeability) and the description of MD transporting process. The model can *simultaneously* solve for the MD processes vapor flux and membrane effective surface temperatures, contrary to other models in which one of them has to be given in order to solve for the other. We argue that this Monte Carlo simulation model can adequately describe MD processes transport phenomenon and predicts process vapor flux without resorting to any adjustable parameters. It is comprehensive in its approach; and it can be applied to all configurations of MD processes published in the literature. The results obtained, in general, show an excellent *qualitative* agreement with available experimental data.

Keywords: Monte carlo; Direct contact membrane distillation; Network model; Heat and mass transfer; Temperature polarization

1. Introduction

Direct contact membrane distillation (DCMD) is one form of membrane distillation (MD) processes in which liquid feed and liquid permeate solution are always in direct contact with the membrane surface. It uses hydrophobic microporous membranes, and therefore, only water vapor and volatile components transport through the membrane pores, while non-volatile components remain in the feed solution. The non-wettability criterion of hydrophobic membrane prevents liquid penetration of feed solution into membrane pores. DCMD process is a thermally driven separation process, operates on the principle of vapor–liquid equilibrium (VLE) conditions, and it is characterized by simultaneous heat and mass transfer. This process has been applied for many areas of industrial interest of aqueous solutions or pure water, such as, the perpetration of ultra-pure water, water desalination, waste water treatment, pharmaceutical industry, and concentration of acids, juices, and salt solutions [1–4].

MD processes, in general, are thermal driven separation processes. The driving force for vapor flux is the vapor pressure gradient across the membrane pores; this difference in vapor pressure is a result of difference in composition and/or temperature of solution in the layers adjoining the membrane surfaces. When the feed solution is pure water or the solute concentration in the aqueous solution is very low, solution vapor pressure at the liquid–vapor interface is governed by fluid temperature adjacent to the membrane surface. These interfacial temperatures ($t_{s,f}$ and $t_{s,p}$) are often differ significantly from measured feed and permeate temperatures ($t_{b,f}$ and $t_{b,p}$). Their values cannot be measured directly, and they are significantly affected by applied membrane physical

* Corresponding author. Tel.: +1 613 562 5800x6114; fax: +1 613 562 5172.
E-mail address: abdussalam_o@hotmail.com (A.O. Imdakm).

0376-7388/$ – see front matter © 2005 Elsevier B.V. All rights reserved.
doi:10.1016/j.memsci.2005.05.026

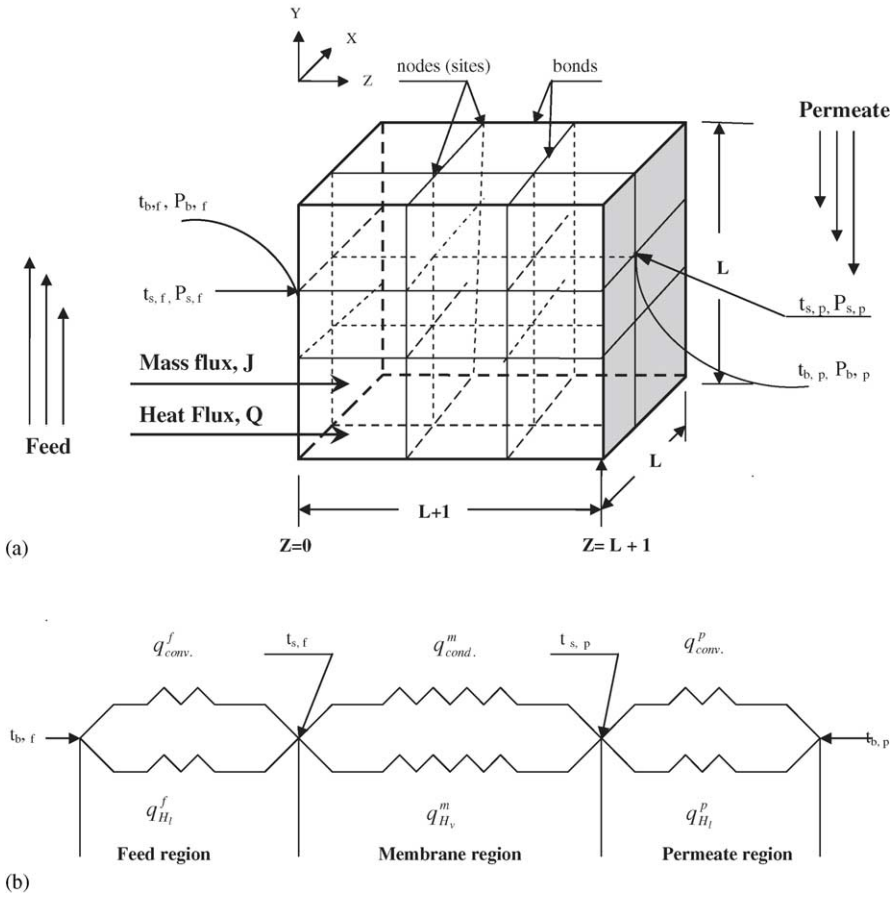

Fig. 1. (a) A schematic heat and mass transfer through hydrophobic membrane (network model of bonds and sites) in DCMD process and (b) DCMD process heat transfer mode electrical analogy [11].

properties and interfacial film heat transfer coefficients h_f and h_p (process dynamics).

DCMD process membrane–bulk interfacial temperatures have received a great deal of attention in the literature [6–12]. This phenomenon is known as temperature polarization and the temperature polarization coefficient, τ, in the literatures is defined as

$$\tau = \frac{t_{s,f} - t_{s,p}}{t_{b,f} - t_{b,p}}. \quad (1)$$

The above equation represents the ratio of the thermal driving force that is actually contributing into the transporting process $(t_{s,f} - t_{s,p})$ to that obtained from the temperature measurement of feed and permeate $(t_{b,f} - t_{b,p})$ (see Fig. 1a,b). For well designed and operated DCMD process, τ should approach unity, which would happen when $t_{s,f} \to t_{b,f}$ as $h_f \to \infty$ and $t_{s,p} \to t_{b,f}$ as $h_p \to \infty$.

Early DCMD heat transfer models to evaluate membrane–bulk interfacial temperatures were developed on the assumptions of a linear temperature distribution across the membrane and an associated enthalpy of flow vapor. In these models, the total heat flux throughout the composite membrane, $Q_{mem.}$, is the sum of the heat conducted through the composite membrane (solid and gas) and the latent heat of vaporization, λ. The total heat flux is therefore given by [6–9]:

$$Q_{mem.} = J\lambda + \frac{k_m}{\delta}(t_{s,f} - t_{s,p}), \quad (2)$$

where k_m is the composite membrane thermal conductivity, δ the membrane thickness, and J is the DCMD process vapor flux. In contrast, recent DCMD heat transfer models were derived on the assumptions of nonlinear temperature distribution across the membrane and non-isenthalpy of flow vapor. Accordingly, the total heat flux through the composite membrane is given as follows [10–12]:

$$Q_{mem.} = JH_v\{T\} + \frac{k_m}{\delta}\frac{dT}{dZ}, \quad (3)$$

where $H_v\{T\}$ is transporting vapor enthalpy at temperature T, and Z is the distance to the direction of vapor flux. The vapor flux, J, is either measured experimentally [8,11,12] or calculated by different vapor flux models available in the literature, such as dusty-gas model (DGM) [13] and Schofield et al. model [7]. However, in many cases, the vapor flux is calculated by the simplest form of vapor flux, which is given as a linear function of vapor pressure difference across the

membrane such as [5,6,10]:

$$J = C(P_f - P_p), \quad (4)$$

where P_f and P_p is the vapor pressure of transporting fluid at the membrane feed and permeate side, respectively, and C is the membrane distillation coefficient that is a function of membrane physical properties (pore size, porosity, thickness, and membrane pore tortuosity), transporting fluid physical properties (molecular weight and diffusivity), and operating temperature. Once the vapor flux, J, is obtained, it is substituted into the equations of heat transfer to evaluate membrane effective surface temperatures. The calculation of membrane surface temperatures in many cases is carried out iteratively [10–12]. The heat fluxes across the membrane boundary layers Q_{feed} and $Q_{per.}$ are usually given as

$$Q_{feed} = h_f(t_{b,f} - t_{s,f}), \quad (5)$$

and

$$Q_{per.} = h_p(t_{s,p} - t_{b,p}), \quad (6)$$

neglecting heat transfer associated with liquid solution enthalpies of feed and permeates ($H_l\{T\}$).

In this study, we have developed a Monte Carlo (MC) simulation model to describe MD transporting processes and to predict process vapor flux (permeability), taking into consideration the effect of process temperature polarization phenomenon. To demonstrate this model capability, it was applied to a specific MD separation process, namely, direct contact membrane distillation (DCMD) process. In this model, the composite membrane is represented by a three-dimensional network model of interconnected pores (bonds) and nodes (sites). The network pores (bonds) represent membrane pore space (pore throats), connected together with network nodes (sites) which represent porous membrane pore bodies. The network pores (bonds), in general, can have any shape and size, but for practical reason, they are usually assumed to be cylindrical of constant length, l, representing average porous membrane pore length, and effective distributed pore radii. The vapor flux through membrane pores was described by gas transport mechanisms founded on the kinetic theory of gases for a single cylindrical tube [18]. In this investigation, we discuss the influence of membrane physical properties, such as, membrane pore size distribution, thickness, porosity, and thermal conductivity on DCMD transporting phenomenon. The role of process dynamics variation (module design) in process performance and process vapor flux prediction will be discussed in detail in future publication.

2. Theory

In this study, Monte Carlo simulation method is applied to describe DCMD transporting process. In MC simulation approach applied in the previous studies, the disorder porous media, in general, is either described by network (discrete) models of inter-connected bonds and sites, or by continuum models which generally ignore the detailed description of the porous media. In this investigation, the pore space of the porous media (porous membrane) is described by a random network model of inter-connected bonds and sites. This means the transporting process is described by finite samples, and therefore, several independent realizations of the simulated transporting process have to be generated, and the results obtained are the average values of transport properties of interest among all these realizations. The number of realizations needed depends on the size of the sample and the required calculation accuracy. For more detailed descriptions of the MC simulation method, computer generation of pore space network models, and the application of MC simulation method in many areas of transport processes, see, for example, Imdakm and Sahimi [15], and Sahimi et al. [17] and references therein.

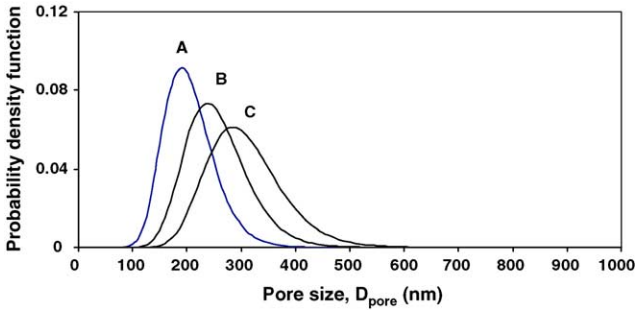

Fig. 2. Probability density function curves for membranes A (μ = 200 nm), B (μ = 250 nm) and C (μ = 300 nm), with a constant (σ = 1.25).

Fig. 1a shows a schematic diagram of vapor flux across the hydrophobic membrane in the DCMD process. The hot and cold layers adjoining the membrane are assumed to be always in direct contact with the membrane surfaces, and therefore, process vapor flux is controlled by formed membrane–bulk interfacial temperatures, $t_{s,f}$, and $t_{s,p}$. The hydrophobic porous membranes pore space is represented by a three-dimensional network model (simple cubic ($L \times L \times L$)) of interconnected bonds and sites, the network size, L, in all cases discussed in this study, is selected such that $L \gg \xi_p$, where ξ_p is percolation correlation length [16]. The network boundaries are ($L \times L$) and represent feed side at $Z = 0$, and permeate side at $Z = L + 1$. These boundaries are assumed to be exposed to DCMD process operating boundary conditions, $t_{s,f}$ and $P_{s,f}$ at the feed side and $t_{s,p}$ and $P_{s,p}$ at the permeate side. The detailed description of network model formulation, including membrane pore size distribution and vapor flux transport mechanism(s) governing vapor flux through membrane pores are discussed by Imdakm and Matsuura [14]. The geometrical pore sizes, standard deviations and the corresponding probability density curves for three membranes used in this study (A, B, and C) are given in Fig. 2.

The complex relation of heat flux, Q, and DCMD process vapor flux, J, for any region shown in Fig. 1b can be written

in general as follows [11,12]:

$$Q = JH\{T\} + h\,\Delta T, \tag{7}$$

where $H\{T\}T$ is transporting fluid enthalpy at temperature T, h the heat transfer coefficient, and ΔT is the temperature drop. Eq. (7) can describe energy flux in these three distinct regions, feed, membrane, and permeate shown in Fig. 1b. Thus, for membranes' feed and permeate side, Eq. (7) becomes:

$$Q_{\text{feed}} = q^{\text{f}}_{H_{\text{l}}} + h_{\text{f}}(t_{\text{b,}} - t_{\text{s,f}}), \tag{8}$$

and

$$Q_{\text{per.}} = q^{\text{p}}_{H_{\text{l}}} + h_{\text{p}}(t_{\text{s,p}} - t_{\text{b,}}), \tag{9}$$

here $q^{\text{f}}_{H_{\text{l}}}$ and $q^{\text{p}}_{H_{\text{l}}}$ are the heat flux because of water liquid transport across feed and permeate boundaries, respectively, both of them equal to $JH_{\text{l}}\{T\}$, where J is DCMD process vapor flux and $H_{\text{l}}\{T\}$ is liquid water enthalpy at temperature T of interest (at feed or permeate side), and it is approximated by

$$H_{\text{l}}\{T\} = -1117.8 + 4.0312T + 2.0 \times 10^{-4}T^2. \tag{10}$$

The above equation is determined from the enthalpy data fitting for water liquid given in thermodynamic property table [20] in the temperature range of 273–373 K. Water liquid enthalpy, $H_{\text{l}}\{T\}$, is evaluated at the mean temperature of bulk and surface temperature of concern (permeate or feed) such as: $(T_{\text{bulk}} + T_{\text{surf.}})/2$. However, any other temperature average can be used. The convection heat transfer across the feed–membrane interface, $h_{\text{f}}(t_{\text{b,f}} - t_{\text{s,f}})$, is defined as $q^{\text{f}}_{\text{conv.}}$, while at the permeate side, $h_{\text{p}}(t_{\text{s,p}} - t_{\text{b,p}})$ is defined as $q^{\text{p}}_{\text{conv.}}$. The heat transfer coefficients, h_{f} and h_{p}, are membrane boundaries heat transfer coefficients. These heat transfer coefficients can be calculated by means of dimensionless Nusselt number, Nu, which is in most of the time estimated from experimentally determined empirical correlations depending on DCMD process module design (process dynamics).

In this model heat transfer analysis, $Q_{\text{mem.}}$ is defined as the total heat transferred across the composite membrane, and at steady state condition, it is equal to Q_{feed} transmitted across the membrane–bulk interface at the feed side and it is also equal to $Q_{\text{per.}}$ dissipated at membrane–bulk interface at the permeate side, assuming no heat losses to the surrounding (Fig. 3). $Q_{\text{mem.}}$ can be described by the following heat transfer mechanisms: (a) heat conducted through membrane material solid phase (polymer) in direct contact with the liquid feed ($q^{\text{m}}_{\text{solid}}$), (b) heat transfer conducted through vapor phase occupying membrane entrance pores ($q^{\text{m}}_{\text{pore}}$), and (c) heat input to the membrane because of saturated water vapor flowing through membrane pores ($q^{\text{m}}_{H_{\text{v}}}$). Although, these heat transfer mechanisms consider only the heat transfer (input) from interfacial feed–membrane layer, corresponding to $Z = 0$ to the adjacent layer, corresponding to $Z = 1$, this heat should eventually be transferred across the entire thickness of the membrane. Thus, the total heat transferred across the composite membrane, $Q_{\text{mem.}}$, is

$$Q_{\text{mem.}} = q^{\text{m}}_{H_{\text{v}}} + q^{\text{m}}_{\text{pore}} + q^{\text{m}}_{\text{solid}}. \tag{11}$$

In the above equation, $q^{\text{m}}_{H_{\text{v}}}$ can be written as $q^{\text{m}}_{H_{\text{v}}} = JH_{\text{v}}\{T\}$, where $H_{\text{v}}\{T\}$ the enthalpy of saturated water vapor at temperature T, and can be approximated by the following equation:

$$H_{\text{v}}\{T\} = 1850.7 + 2.8273T - 1.6 \times 10^{-3}T^2 \tag{12}$$

This equation of $H_{\text{v}}\{T\}$ is also determined from the enthalpy data fitting for saturated water vapor given in thermodynamic property table [20] in the same temperature range mentioned above. $H_{\text{v}}\{T\}$ is evaluated at temperature T of interest, which is in this investigation assumed to be equal to the mean temperature of feed temperature and feed–membrane interfacial temperature, $(T_{\text{b,f}} + T_{\text{s,f}})/2$. The second term in Eq. (11), $q^{\text{m}}_{\text{pore}}$, is the total heat conducted through the vapor occupying membrane entrance pores in direct contact with the feed (at $Z = 0$), assuming creeping flow across the entire membrane pores, i.e., ignoring convection heat transfer, although it can be included if necessary, $q^{\text{m}}_{\text{pore}}$ can be written as

$$q^{\text{m}}_{\text{pore}} = \frac{k_{\text{v}}}{A_{\text{s}}l}\sum_{n=1}^{L^2}\left(t_{\text{s,f}} - t_{n,2}\right)\pi r^2_{n\text{k}}, \tag{13}$$

where k_{v} is the transporting vapor thermal conductivity, l the average membrane pore length, A_{s} is membrane interfacial surface area, $r_{n\text{k}}$ the entering pore radius attached to nth node at network first section, corresponding to $Z = 0$, and $t_{n,2}$ is the temperature of the nth node at network second section,

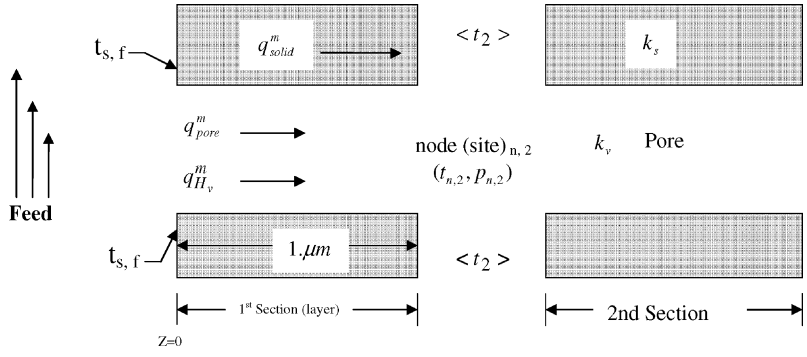

Fig. 3. Heat transfer through composite membrane solid phase (polymer) and vapor phase (occupying membrane entering pores) in direct contact with the feed.

corresponding to $Z = 1$ as shown in Fig. 2. The summation is carried out for the entire network entering pores at $Z = 0$. The third term is the energy conducted across membrane solid phase (polymer) in direct contact with the feed, q^{m}_{solid}, it can be calculated by the following equation:

$$q^{m}_{solid} = \frac{k_s}{l}(t_{s,f} - \langle t_2 \rangle)(1 - S_p) \quad (14)$$

where $t_{s,f}$ represents membrane–bulk interfacial temperature at the feed side and $\langle t_2 \rangle$ is the average nodal temperatures of the network second section (layer), which is defined as $\sum_{n=1}^{L^2} t_{n,2}/L^2$. Note that in this model, the conduction heat transfer across the composite membrane is the sum of heat conducted across both membrane solid phase (polymer) in direct contact with the feed and the vapor phase occupying membrane entrance pores. In both cases the thermal conductivities can be measured independently. In the past modeling, in order to calculate the heat flux across the composite membrane, one had to calculate the effective thermal conductivity of the composite membrane, k_m. This, however, is difficult to measure independently, and therefore, it is usually estimated from vapor and solid phase thermal conductivities such as: $k_m = \varepsilon k_v + (1 - \varepsilon)k_s$ [6–12], where ε is the composite membrane porosity.

As can be seen, all MD processes are in fact boundary value problems, i.e., in order to solve for process vapor flux and interfacial surface temperatures, membrane boundaries (feed and permeate) bulk temperatures, $t_{b,f}$ and $t_{b,p}$, and heat transfer coefficients, h_f and h_p, have to be defined. All MD processes, regardless of their different configurations, share the same feed side process setup, which is the assumption of liquid feed in direct contact with feed side membrane surface, and therefore heat flux descriptions, Q_{feed} and $Q_{mem.}$, applied in DCMD feed and membrane regions (see Fig. 1b), can be applied to all MD processes. Hence, the difference in heat flux and mass flux descriptions may occur at MD processes permeate side only; depending on each MD process permeate side setup. These differences in heat and vapor flux transport mechanism(s) at the permeate side may vary in the details from one process to another, but in general the total heat flux across the permeate region, $Q_{per.}$, can be described by the same general form of energy flux, $Q = JH\{T\} + h\Delta T$, discussed above. Therefore, this MC simulation model developed in this study, can be applied to all MD processes regardless of their different configurations, taking into consideration these possible differences in mass and energy flux transport mechanism(s) which may occur at the permeate side.

3. Calculation procedure

Once the geometrical configuration of the membrane, DCMD process operating condition(s), and composite membrane physical properties, are given, the steady state heat transfers across membrane boundaries Q_{feed}, and $Q_{per.}$, membrane surface temperatures, $t_{s,f}$, and $t_{s,p}$, and energy input into the composite membrane, $Q_{mem.}$ can be computed iteratively using proper iterative method such as the method of successive substitutions [19]. An initial guess of interfacial membrane surface temperatures, $t_{s,f}$, and $t_{s,p}$, are given, to calculate vapor pressure at network boundaries (feed, and permeate side), using the Antoine equation [16]. Afterward, network nodal pressure and temperature distribution, and the corresponding simulated DCMD process vapor flux, J, can be calculated as discussed by Imdakm and Matsuura [14]. Once process vapor flux is calculated, the energy fluxes, $Q_{mem.}$, Q_{feed}, and $Q_{per.}$ can be calculated as discussed above. As a result, the relative energy error (REE) criterion, which is defined as: $\text{REE} = Q_{feed} - Q_{mem}/Q_{feed}$ can be determined, assuming no energy losses to the surrounding. If REE exceeds or becomes equal to 2%, membrane surface temperatures, $t_{s,f}$ and $t_{s,p}$, are re-calculated using recently computed feed side interfacial temperature $(t_{s,f})_m$, such as: $(t_{s,f})_{m+1} = (t_{s,f})_m + \text{REE}$, and the corresponding $t_{s,p}$ can be calculated using Eqs. (8) and (9). Note that $\text{REE} \to 0$ as $t_{s,f}$ and $t_{s,p}$ approaches their steady state values. This calculation procedure is repeated until the relative energy error (REE) becomes below 2%. Once the relative error in the heat transfer rate becomes less than 2%, one can assume that the computed interfacial temperatures, $t_{s,f}$ and $t_{s,p}$, and nodal vapor pressure and temperature distribution across the entire network, are the steady state values required for the simulated DCMD process. And therefore, the resulting temperature polarization coefficient, τ, and vapor flux, J, respectively, the temperature polarization coefficient and the vapor flux of the simulated DCMD process at steady state condition.

4. Results of Monte Carlo simulation

The model was applied for DCMD process in which water vapor is assumed to be the only permeate, as in the desalination of brackish and seawater. Therefore, the value of transporting vapor thermal conductivity, k_v, is assumed to be that of water vapor, $0.02\,\text{W m}^{-1}\,\text{K}^{-1}$, in this work [12]. The influence of the following membrane physical properties is investigated because of their important effects on MD transporting process: membrane pore size distribution (A and C), pore level vapor flux transport mechanism(s), membrane thickness, membrane surface porosity, and composite membrane solid phase (polymer) thermal conductivity. These studies were carried out under different feed temperatures in a range of 40–90 °C, permeate temperature of 20 °C, heat transfer coefficient of $15{,}000\,\text{W m}^{-2}\,\text{K}^{-1}$at the feed side, h_f, and at the permeate side, h_p, composite membrane surface porosity, S_p, of 3.5%, membrane solid phase (polymer) thermal conductivity, k_s, of $0.04\,\text{W m}^{-1}\,\text{K}^{-1}$, and network size, $L = 12$, unless they are specified differently. The transport properties reported, for all cases discussed in this study, are averaged over 20 realizations.

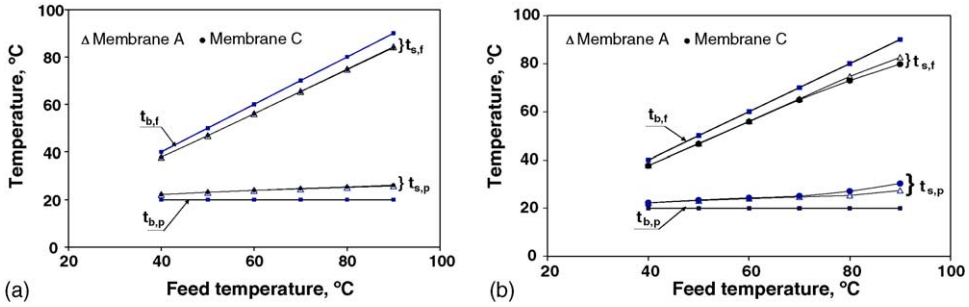

Fig. 4. Comparison of simulated DCMD process interfacial membrane surface temperatures ($t_{s,f}$ and $t_{s,p}$) with bulk temperatures ($t_{b,f}$ and $t_{b,p}$) for membranes A and C. (a) Process is controlled by Knudsen diffusion only and (b) process is controlled by Knudsen diffusion and viscous flow; h_f and $h_f = 15{,}000\ W\,m^{-2}\,K^{-1}$, and $S_p = 3.5\%$.

4.1. Effect of membrane pore size distribution

Fig. 4 shows membrane–bulk interfacial surface temperatures, $t_{s,f}$, and $t_{s,p}$, versus feed temperature for membrane A and C. When the DCMD process is controlled only by Knudsen diffusion only Fig. 4a, this figure shows, the decrease of $t_{s,f}$ and the increase of $t_{s,p}$ because of pore size increases is only of a few degrees, i.e. the pore size distribution has practically no significant effect. However, when viscous flow is taken into consideration, Fig. 4b shows $t_{s,f}$ decreases while $t_{s,p}$ increases significantly as pore sizes increase, from A to C. This is probably due to the increase of the fraction of pores governed by viscous flow as the membrane pore size increases (see Fig. 6).

Fig. 5 shows the results of vapor flux calculation as a function of feed temperature for the following two cases; when temperature polarization phenomenon was taken into consideration and when it was neglected (with h_f and h_p equal to infinity). Although results for membrane B are not shown, they were between A and C. Fig. 4a,b reveals that feed–membrane interfacial temperature, $t_{s,f}$, is always less than $t_{b,f}$ when temperature polarization phenomenon is taken into consideration. As a result, the vapor pressure at the feed–membrane interface is lower than the vapor pressure at the feed bulk, which results in lower vapor flux as observed in Fig. 5. This effect is seen most clearly when the transporting process is controlled by Knudsen diffusion only (Fig. 5, solid line).

Let us now consider the case when the viscous flow is taken into consideration (Fig. 5, broken line). When h_f and h_p decrease from infinity to $15{,}000\ W\,m^{-2}\,K^{-1}$, or in other words when there is a temperature polarization effect, $t_{s,f}$ becomes lower than $t_{b,f}$ which should result in a decrease in process vapor flux. On the other hand, this decrease in $t_{s,f}$ causes also a decrease in the fraction of pores governed by viscous flow, particularly in the vicinity of the feed–membrane interface [14] (see also Fig. 6), which should cause an increase in the vapor flux. These two conflicting effects will counteract with each other and the fluxes with and without temperature polarization will eventually meet. It is more obvious when the feed temperature is high and the average pore size is large (see Fig. 5, broken line).

Fig. 7 shows temperature polarization coefficient, τ, versus feed temperature. As can be seen, when the DCMD process is controlled by Knudsen diffusion only, it increases slightly as feed temperature increase. However, when the transporting process is controlled by Knudsen diffusion and viscous flow, it declines, and the declining rate clearly depends on the fraction of network pores governed by viscous

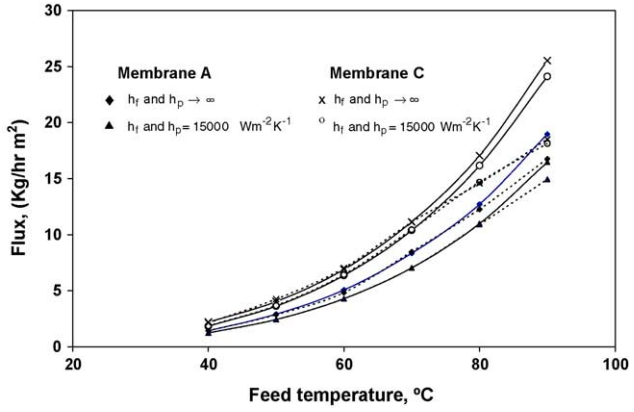

Fig. 5. Comparison of simulated DCMD vapor flux for membrane A and C: (—) process is controlled by Knudsen diffusion only; (- - -) process is controlled Knudsen diffusion and viscous flow; $S_p = 3.5\%$.

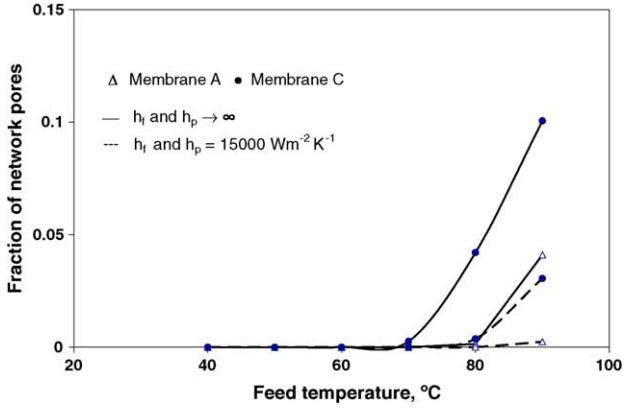

Fig. 6. Comparison of simulated DCMD process fraction of network pores governed by viscous flow for membrane A and C; $S_p = 3.5\%$.

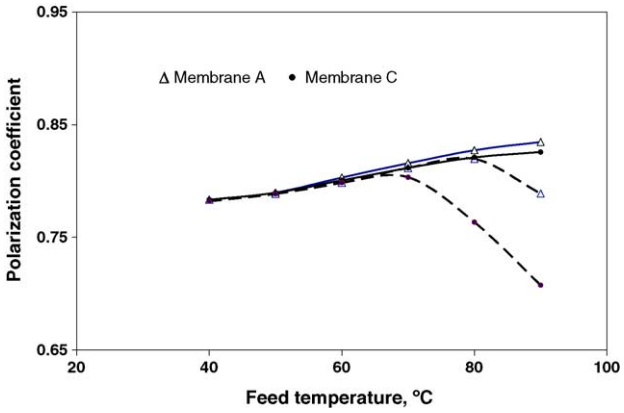

Fig. 7. Comparison of simulated DCMD temperature polarization coefficient, τ, for membranes A and C: (—) process is controlled by Knudsen diffusion and (- - -) process is controlled by Knudsen and viscous flow; h_f and $h_p = 15{,}000\ W\,m^{-2}\,K^{-1}$ and $S_p = 3.5\%$.

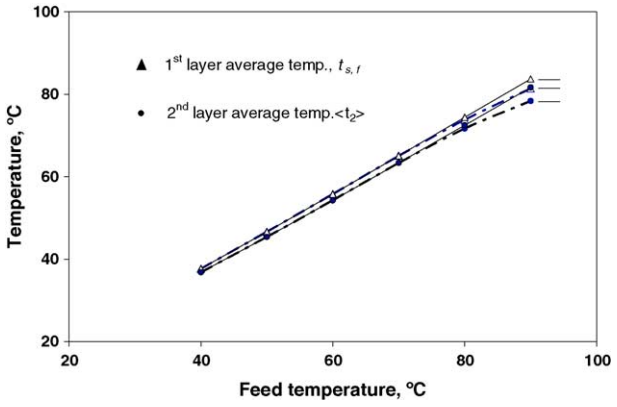

Fig. 9. Average temperatures of first and second network layers (sections), for membrane B: (—) process is controlled by Knudsen diffusion and (- - -) process is controlled by Knudsen and viscous flow; h_f and $h_p = 15{,}000\ W\,m^{-2}\,K^{-1}$ and $S_p = 3.5\%$.

flow, i.e. comparing broken lines of Figs. 6 and 7 for which calculation was done under identical condition, it is quite obvious that the decrease in polarization coefficient coincided with the increase in the fraction of network pores governed by viscous flow.

Fig. 8a,b shows the percentage of the heat transferred due to mass transfer across feed side thermal boundary layer ($\%q^f_{H_l}$) and the heat transferred due to vapor flux through membrane pores ($\%q^m_{H_v}$) with respect to the steady state total energy transferred across the composite membrane. Looking into the solid lines, these figures indicate that both $\%q^f_{H_l}$ and $\%q^m_{H_v}$ increase monotonically with feed temperature, when the process is controlled by Knudsen diffusion only. As well they increase with an increase in the pore size distribution from A to C, because of their dependency on process vapor flux, J. But $q^f_{H_l} \ll q^m_{H_v}$, and the difference between these two quantities increases with the increase of feed temperature, meaning more thermal energy has to be supplied from the feed across feed–membrane interface to evaporate the liquid, which further leads to a decrease of $t_{s,f}$ The same thermal energy has to be dissipated at the permeate side, resulting in an increase in $t_{s,p}$. Hence the polarization coefficient defined by Eq. (1) should decrease. Although this trend is not seen in Fig. 7, when only Knudsen diffusion is considered (solid line), it will eventually occur when membrane surface porosity, S_p, is much greater than 3.5%, as it will be illustrated in Fig. 13.

4.2. Effect of viscous flow transport mechanism (viscous effect)

Inclusion of viscose flow transport mechanism reduces process vapor flux (see Fig. 5, broken line), and $q^m_{H_v}$ and $q^f_{H_l}$ because of their dependency on process vapor flux. Therefore, the energy demand for liquid evaporation from the feed (convection) should decrease. As a result, $t_{s,f}$ should increase, $t_{s,p}$ should decrease, and an increase of temperature polarization coefficient, τ, should be observed. But what actually happens, throughout all cases discussed in this study, is a decline of temperature polarization coefficient, as can be seen in Fig. 7 (from solid to broken lines). This rather unexpected phenomenon can be explained by considering conduction heat transfer across the membrane, $q^m_{cond.}$, which is the sum of q^m_{pore} and q^m_{solid}. Let us look into Fig. 9 where the average temper-

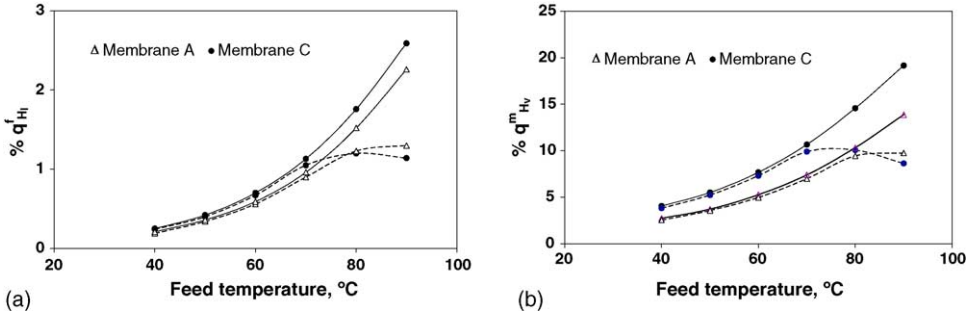

Fig. 8. Comparison of percentage of energy transported by (a) liquid water enthalpy, $q^f_{H_l}$, and (b) saturated water vapor enthalpy, $q^m_{H_v}$, for membrane A, and C: (—) process is controlled by Knudsen diffusion, and (- - -) process is controlled by Knudsen and viscous flow; h_f and $h_p = 15{,}000\ W\,m^{-2}\,K^{-1}$, and $S_p = 3.5\%$.

ature of the feed–membrane interface ($t_{s,f}$), corresponding to $Z = 0$, and that of the adjacent layer ($\langle t_2 \rangle$), corresponding to $Z = 1$, are plotted versus feed temperature. Solid lines are again for the case where only Knudsen diffusion is considered while the broken lines are for the case where both Knudsen diffusion and the viscous flow are considered. This figure shows clearly that the average temperature at $Z = 0$ (shown by △) is higher than at $Z = 1$ (shown by ●), and the difference between these two layers becomes greater when both Knudsen diffusion and viscous flow are considered. Taking into consideration that the temperature drop and pressure drop from $Z = 0$ to $Z = 1$ are interrelated by the Antoine equation [16], the greater temperature decrease observed above seems due to the greater mass transfer resistance that occurs when viscous flow is included.

The greater temperature difference between the interfacial layer ($Z = 0$) and the adjacent layer ($Z = 1$) means an increase in conduction heat transfer across the membrane. This increase in conduction heat transfer through the membrane, $q^{m}_{cond.}$, when viscous flow is included into the transporting process, will be possible only by an increase in convection heat transfer, $q^{f}_{conv.}$, across feed–membrane interface, which in turn lowers interfacial temperature, $t_{s,f}$. (Note that contribution of $q^{f}_{H_l}$ is only few percent of the total heat flux). Similarly, $t_{s,p}$ will increase, resulting in a decrease in temperature polarization coefficient, τ, as shown in Fig. 7.

4.3. Effect of membrane thickness, L'

To simulate the effect of increasing membrane thickness on the DCMD process performance, a Monte Carlo simulation procedure was carried out using network model of varies sizes. This is accomplished by varying network size in the direction of flow, Z. Hence, the dimension of the network model, in this case, is modified to ($L \times L \times L'$), L' varied in the Z-direction (direction of flow) from L to $3L$, and $L = 10$. The reduction of network size in X and Y direction (from $L = 12$ to $L = 10$) was necessary in order not to exceed available computer memory due to L' increase in Z-direction. The solid lines in Fig. 10 shows that process vapor flux decrease, approaching an asymptotic value as L' increases. On the other hand, solid lines in Fig. 11 shows that the temperature polarization coefficient increases as L' increases from 10 to 15 and then level off, which is the reflection of the vapor flux curves of Fig. 10. When the transporting process is controlled by Knudsen diffusion only, as the vapor flux decreases, the heat transfer across feed–membrane interface also decrease, which brings up the interfacial temperature $t_{s,f}$ and brings down $t_{s,p}$. As a result, temperature polarization coefficient, τ, will increases (Fig. 11, solid line). When the viscous flow is added to the Knudsen diffusion, the vapor flux decreases (Fig. 10, broken lines as compared with solid lines), and the resulting temperature polarization coefficient decrease (see Fig. 11, broken line) is due to viscous flow effect discussed above. However, as L' increases, both vapor flux and temperature polarization coefficients level off because

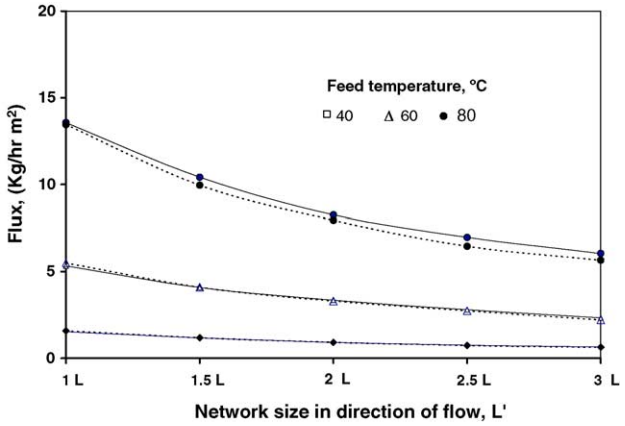

Fig. 10. Simulated DCMD vapor flux vs. membrane thickness, L', for membrane B: (—) process is controlled by Knudsen diffusion only and (- - -) process is controlled by Knudsen and viscous flow; h_f and $h_p = 15{,}000\ W\ m^{-2}\ K^{-1}$, and $S_p = 3.5\%$, $L = 10$.

of diminishing effect of pressure drop, and temperature drop as well, across the membrane layers on both process vapor flux and heat transport. It is very interesting to note that temperature polarization coefficient (interfacial temperatures), process vapor flux and the fraction of pores governed by viscous flow approach asymptotic values of diminishing dependency on membrane thickness, L', as membrane thickness increases.

4.4. Effect of porous membrane surface porosity, S_p

Fig. 12 shows increase of vapor flux with the increase in membrane surface temperature, S_p, resulting in an increase of $q^{f}_{H_l}$ and $q^{m}_{H_v}$ as discussed above, and therefore, the temperature polarization coefficient decreases as S_p increases (see Fig. 13, solid line). When viscous flow is taken into consideration Fig. 12 shows a slight decrease in vapor flux (broken

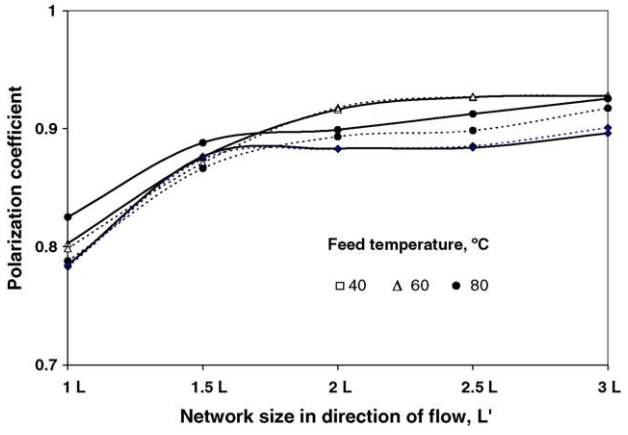

Fig. 11. Simulated DCMD temperature polarization coefficient, τ, vs. membrane thickness, L', for membrane B: (—) process is controlled by Knudsen diffusion only, and (- - -) process is controlled by Knudsen diffusion and viscous flow; h_f and $h_p = 15{,}000\ W\ m^{-2}\ K^{-1}$, $S_p = 3.5\%$, and $L = 10$.

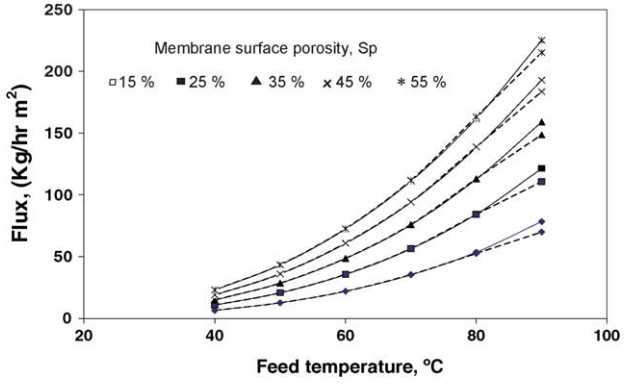

Fig. 12. Simulated DCMD vapor flux dependency on membrane surface porosity, S_p, for membrane B: (—) process is controlled by Knudsen, and (- - -) process is controlled by Knudsen and viscous flow; h_f and $h_p = 15{,}000\ W\,m^{-2}\,K^{-1}$.

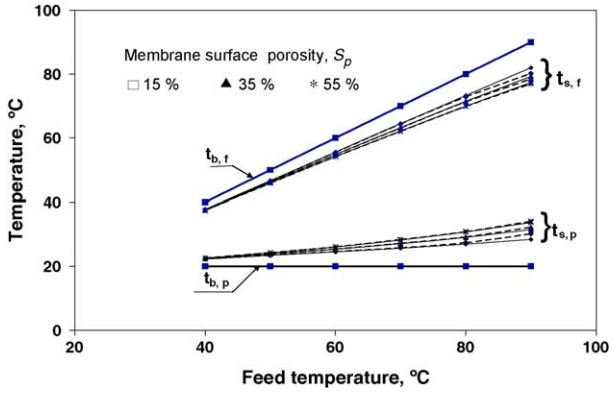

Fig. 14. Variation of simulated DCMD membrane interfacial surface temperatures, ($t_{s,f}$, and $t_{s,p}$), with the change of membrane surface porosity, S_p, for membrane B: (—) process is controlled by Knudsen, and (- - -) process is controlled by Knudsen and viscous flow; h_f and $h_p = 15{,}000\ W\,m^{-2}\,K^{-1}$.

line). Fig. 13 shows that the temperature polarization coefficient, τ, decreased slightly also as S_p increases (broken line compared with solid line). This is in accordance with the earlier discussion of the effect of the inclusion of viscous flow on interfacial surface temperature and temperature polarization phenomenon (viscous effect). However, the effect of viscous flow will diminish as membrane surface porosity increases, this is because of the diminishing of heat conducted through membrane solid phase (polymer), q^m_{solid}, due to the decrease of membrane solid phase (polymer) surface area in direct contact with the feed as S_p increases. As a result, temperature polarization coefficient curves when viscous flow is taken into consideration are actually approaching temperature polarization coefficient curves when it was neglected (see Fig. 13), same results observed for interfacial surface temperatures and vapor flux curves as shown in Figs. 12 and 14. The process vapor flux increase with an increase S_p despite the fact that the feed–membrane interfacial temperature, $t_{s,f}$, decreases (see Fig. 14). This increase of the flux is due to the increase of surface area available for vapor flux and the reduction of fraction of pores governed viscous flow as shown in Fig. 15.

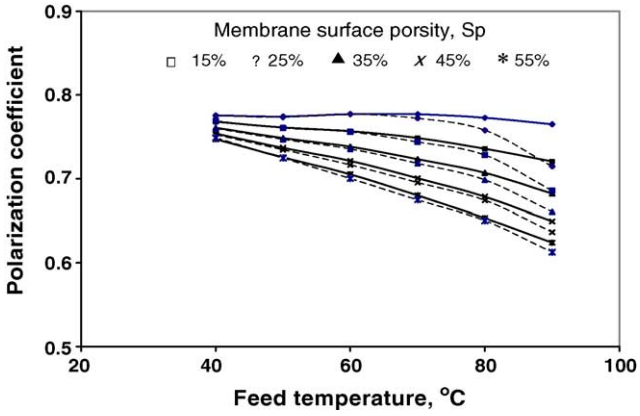

Fig. 13. Variation of simulated DCMD polarization coefficient, τ, with membrane surface porosity for membrane B: (—) process is controlled Knudsen, and (- - -) process is controlled Knudsen and viscous flow; h_f and $h_p = 15{,}000\ W\,m^{-2}\,K^{-1}$.

4.5. *Effect of membrane thermal conductivity, k_s*

The effect of k_s on DCMD membrane performance has been discussed by many investigators [5–12]. The increase of membrane solid phase (polymer) thermal conductivity, k_s, increases composite membrane thermal conductivity, k_m, This will lower MD process vapor flux since q^m_{solid} increases with an increase in k_s, and therefore, most of the heat will be transmitted through membrane solid phase instead of evaporating liquid feed. This was confirmed by the Monte Carlo simulation as shown in Fig. 16. Increasing membrane solid phase thermal conductivity, increases $Q_{mem.}$, reduces $t_{s,f}$ and increases $t_{s,p}$ as shown in Fig. 17, and hence decreases process polarization coefficient (see Fig. 18). Inclusion of viscous flow lowers $t_{s,f}$ and process polarization coefficient even further due to the significant increase of $q^m_{cond.}$ (viscous effect), as a result, the fraction of network pores governed by viscous flow decreases as k_s increases (see Fig. 19). This decrease of

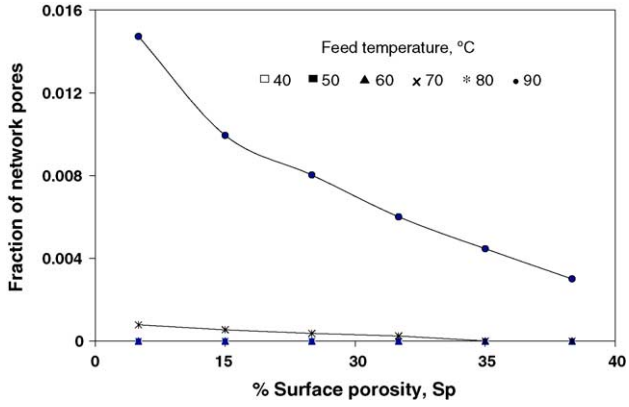

Fig. 15. Dependency of simulated DCMD fraction of pores governed by viscous flow on the variation of membrane surface porosity, S_p, for membrane B; h_f and $h_p = 15{,}000\ W\,m^{-2}\,K^{-1}$.

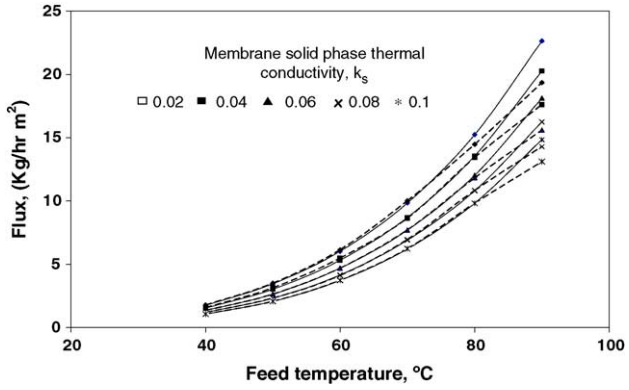

Fig. 16. Variation of simulated DCMD vapor flux with the change of membrane polymer thermal conductivity, k_s, for membrane B: (—) process is controlled by Knudsen diffusion, and (- - -) process is controlled by Knudsen diffusion and viscous flow; h_f and $h_p = 15{,}000\ W\,m^{-2}\,K^{-1}$, and $S_p = 3.5\%$.

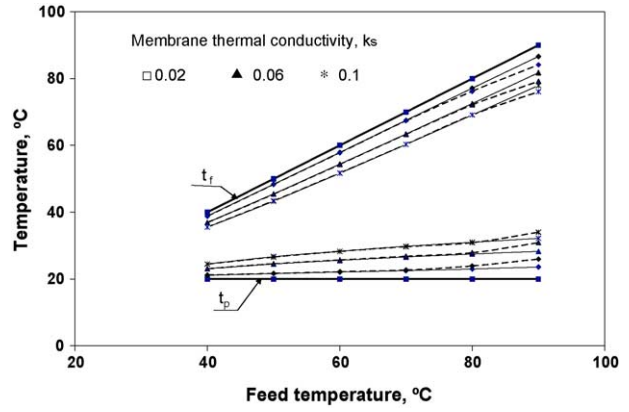

Fig. 17. Variation of simulated DCMD membrane interfacial surface temperatures, ($t_{s,f}$, and $t_{s,p}$), with the change of membrane solid phase (polymer) thermal conductivity, k_s, for membrane B: (—) process is controlled by Knudsen diffusion, and (- - -) process is controlled by Knudsen diffusion and viscous flow; h_f and $h_p = 15{,}000\ W\,m^{-2}\,K^{-1}$, and $S_p = 3.5\%$.

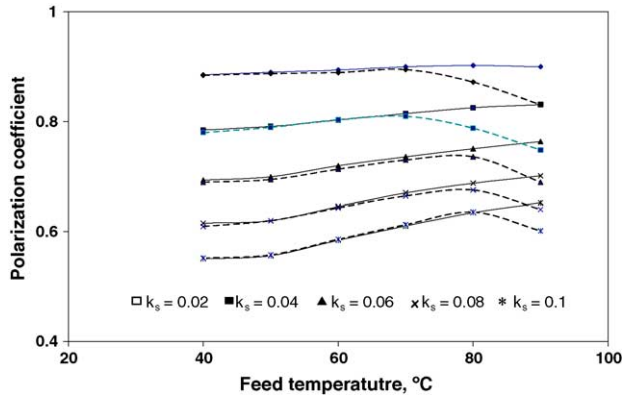

Fig. 18. Variation of simulated DCMD polarization coefficient with the change of membrane solid phase (polymer) thermal conductivity, k_s, for membrane B: (—) process is controlled by Knudsen diffusion, and (- - -) process is controlled by Knudsen diffusion and viscous flow; h_f and $h_p = 15{,}000\ W\,m^{-2}\,K^{-1}$, and $S_p = 3.5\%$.

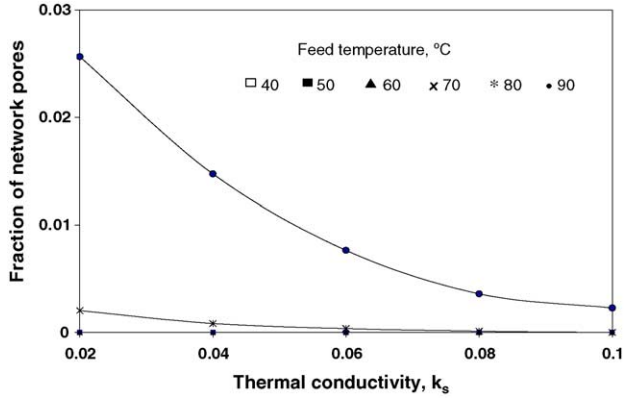

Fig. 19. Variation of simulated DCMD fraction of network pores governed by viscous flow with the change of membrane solid phase (polymer) thermal conductivity, k_s, for membrane B; h_f and $h_p = 15{,}000\ W\,m^{-2}\,K^{-1}$, and $S_p = 3.5\%$.

fraction of pores governed by viscous flow should cause an increase of the vapor flux, but its effect on process vapor flux was not as strong as the effect of $t_{s,f}$ reduction.

5. Summery and conclusion

In this investigation, a Monte Carlo (MC) simulation model was developed for membrane distillation (MD) processes. This model is comprehensive in its approach and can be applied to all forms of MD processes published in the literature regardless of their different configurations. As an example of this model capability, it was applied to a specific MD separation process, such as, direct contact membrane distillation process (DCMD) to describe process performance and process vapor flux prediction, taking into account the effect of temperature polarization phenomenon, porous membrane physical properties, including membrane pores interconnectivity (topology), process dynamics, and pore level vapor flux transport mechanism(s). This MC model can predict *simultaneously* process vapor flux (permeability) and membrane effective surface temperatures, taking into consideration their mutual effects in the transporting process. This step is a significant advancement in MD simulation compared with other models in which either process vapor flux or effective membrane surface temperatures has to be given in order to predict the other. Results obtained show that this model can describe MD transporting processes and in detail without the need for any adjustable parameter(s), and therefore, this model will enhance significantly our understanding of MD transporting processes and it may play a supportive role to experimental work, optimizing membrane structuring and MD process module design (process dynamics). The results obtained in this study, in general, show an excellent *qualitative* agreement with available experimental data [8,10,13]. The capabilities of this model in predicting a specific experimental data will be published in the near future.

Acknowledgment

One of us (A. Imdakm) would like to thank Maadani Omran for very useful assistants during the preparation of this work.

Nomenclature

A_s	membrane interfacial surface area (m^2)
C	membrane distillation coefficient ($kg\,m^{-2}\,s^{-1}\,Pa^{-1}$)
D_{pore}	pore diameter (m)
h_f and h_p	heat transfer coefficient at feed and permeate side ($W\,m^{-2}\,K^{-1}$)
$H_l\{T\}$	liquid water enthalpy at temperature T ($kJ\,kg^{-1}$)
$H_v\{T\}$	saturated vapor water enthalpy at temperature T ($kJ\,kg^{-1}$)
J	vapor flux ($kg\,m^{-2}\,h^{-1}$)
k_m	composite membrane effective thermal conductivity ($Wm^{-1}\,K^{-1}$)
k_s	membrane solid phase (polymer) thermal conductivity ($Wm^{-1}\,K^{-1}$)
k_v	membrane vapor phase (water vapor) thermal conductivity ($Wm^{-1}\,K^{-1}$)
l	pore length (1 μm)
L	network size (number of nodes (sites))
L'	network size in the direction of flow, Z, (number of nodes (sites))
Nu	Nusselt number
$P_{b,f}$ and $P_{b,p}$	vapor pressure at feed and permeate side (Pa)
$P_{s,f}$ and $P_{s,p}$	vapor pressure at membrane-feed and membrane-permeate interface (Pa)
q^m_{cond}	conduction heat transfer rate across membrane solid phase and vapor phase in direct contact with the feed ($kW\,m^{-2}$).
q^f_{conv}	convection heat transfer rate across membrane-feed interface ($kW\,m^{-2}$).
q^p_{conv}	convective heat transfer rate across membrane-permeate boundary at the permeate side ($kW\,m^{-2}$).
q^m_{Hl}	heat transfer due to liquid flux across membrane-feed boundary layer ($kW\,m^{-2}$)
q^p_{Hl}	heat transfer rate due water flux across membrane-permeate boundary layer ($kW\,m^{-2}$).
q^m_{Hv}	heat transfer due to vapor flowing through membrane pores ($kW\,m^{-2}$)
q^m_{pore}	conduction heat transfer rate across vapor phase occupying entering membrane pores at $Z = 0$ ($kW\,m^{-2}$)
q^m_{solid}	conduction heat transfer rate cross membrane solid phase (polymer) at $Z = 0$ ($kW\,m^{-2}$).
Q_{feed}	total heat transfer rate across membrane-feed boundary ($kW\,m^{-2}$)
$Q_{mem.}$	total heat transfer rate across the composite membrane ($kW\,m^{-2}$)
$Q_{per.}$	total heat transfer rate across membrane-permeate boundary ($kW\,m^{-2}$)
r_{nk}	entering pore radius (attached to the nth node) in direction of flow, Z, (m)
S_p	membrane surface porosity
$t_{b,f}$ and $t_{b,p}$	bulk temperatures at feed and permeate sides (°C), respectively
$t_{s,f}$ and $t_{s,p}$	interfacial membrane-surface temperatures at feed and permeate sides (°C), respectively.
T	temperature (K)
X, Y, and Z	axial coordinates

Greek letters

δ	membrane thickness (m)
ε	composite membrane porosity
λ	latent heat of vaporization ($J\,kg^{-1}$)
μ_{pore}	mean pore size of the pores (m)
ξ_p	percolation correlation length
σ_{pore}	geometrical standard deviation of the pores
τ	temperature polarization coefficient

References

[1] K. Schneider, W. Holz, R. Wollbek, Membranes and modules transmembrane distillation, J. Membr. Sci. 39 (1988) 25–42.
[2] V. Calabro, E. Drioli, F. Matera, Membrane distillation in textile wastewater treatment, Desalination 83 (1991) 209–224.
[3] Y. Wu, Y. Kong, J. Liu, J. Zhang, J. Xu, An experimental study on membrane distillation: crystallization for treating wastewater in taurine production, Desalination 80 (1991) 235–242.
[4] V. Calabro, B.L. Jiao, E. Drioli, Theoretical and experimental study on membrane distillation in the concentration of orange juice, Ind. Eng. Chem. Res. 33 (1994) 1803–1808.
[5] R.W. Schofield, A.G. Fane, C.J.D. Fell, R. Macoun, Factors affecting flux in membrane distillation, Desalination 77 (1990) 279–294.
[6] R.W. Schofield, A.G. Fane, C.J.D. Fell, Heat and mass transfer in membrane distillation, J. Membr. Sci. 33 (1987) 299–313.
[7] R.W. Schofield, A.G. Fane, C.J.D. Fell, Gas and vapor transport through microporous membranes. II. Membrane distillation, J. Membr. Sci. 53 (1990) 173–185.
[8] Marek Gryta, Maria Tomaszewska, Heat transport in the membrane distillation process, J. Membr. Sci. 144 (1998) 211–222.
[9] M.A. Izquierdo-Gil, M.C. Garcia-Payo, C. Fernandez-Pineda, Air gas membrane distillation of sucrose aqueous solutions, J. Membr. Sci. 155 (1999) 291–307.
[10] L. Martinez-Diez, M.I. Vazquez-Gonzalez, Temperature and concentration polarization in membrane distillation of aqueous salt solutions, J. Membr. Sci 156 (1999) 265–273.
[11] Jirachote Phattaranawik, Ratana Jiraratananon, Direct contact membrane distillation: effect of mass transfer on heat transfer, J. Membr. Sci. 188 (2001) 137–143.

[12] J. Phattaranawik, R. Jiraratananon, A.G. Fane, Heat transport and membrane distillation coefficients in direct contact membrane distillation, J. Membr. Sci. 212 (2003) 177–193.
[13] Kevin W. Lawson, Douglas R. Lloyd, Membrane distillation. II. Direct contact MD, J. Membr. Sci. 120 (1996) 123–133.
[14] A.O. Imdakm, T. Matsuura, A Monte Carlo simulation model for membrane distillation processes: direct contact (MD), J. Membr. Sci. 237 (2004) 51–59.
[15] A.O. Imdakm, M. Sahimi, Computer simulation of particles transport processes in flow through porous media, Chem. Eng. Sci. 46 (1991) 1977–1993.
[16] M. Sahimi, A.O. Imdakm, The effect of morphological disorder on hydrodynamic dispersion in flow through porous media, J. Phys. A: Math. Gen 21 (1988) 3833–3870.
[17] Muhammad Sahimi, George R. Gavalas, Theodore T. Tsotsis, Statistical and continuum models of fluid-solid reaction in porous media, Chem. Eng. Sci. 45 (1990) 1443–1502.
[18] R.D. Present, Kinetic Theory of Gases, McGraw-Hill, New York, 1958.
[19] R.G. Rice, D.D. Do, Applied Mathematics and Modeling for Chemical Engineers (Appendix A), Wiley, 1995.
[20] J.M. Smith, H.C. Van Ness, Introduction to Chemical Engineering Thermodynamics, 4th ed., McGraw-Hill, New York, 1987.